This article was downloaded by:
On: *23 January 2011*
Access details: *Access Details: Free Access*
Publisher *Taylor & Francis*
Informa Ltd Registered in England and Wales Registered Number: 1072954 Registered office: Mortimer House, 37-41 Mortimer Street, London W1T 3JH, UK

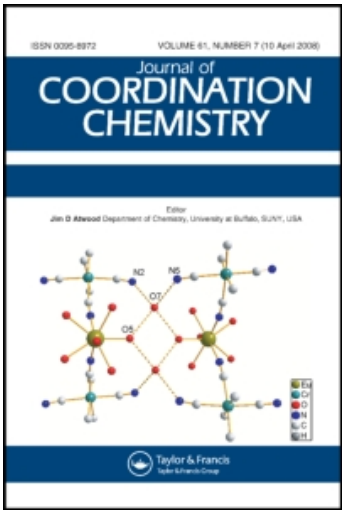

Journal of Coordination Chemistry
Publication details, including instructions for authors and subscription information:
http://www.informaworld.com/smpp/title~content=t713455674

From Planar Toward Tetrahedral Copper(Il) Complexes: Structural and Electron Paramagnetic Resonance Studies of Substituent Steric Effects in an Extended Class of Pyrrolate-Imine Ligands

Chamika M. Wansapura[a]; Choi Juyoung[a]; Jason L. Simpson[a]; Dennis Szymanski[b]; Gareth R. Eaton[b]; Sandra S. Eaton[b]; Stephen Fox[a]
[a] Department of Chemistry, University of Louisiana, Monroe, LA, USA [b] Department of Chemistry and Biochemistry, University of Denver, Denver, CO, USA

Online publication date: 15 September 2010

To cite this Article Wansapura, Chamika M. , Juyoung, Choi , Simpson, Jason L. , Szymanski, Dennis , Eaton, Gareth R. , Eaton, Sandra S. and Fox, Stephen(2003) 'From Planar Toward Tetrahedral Copper(Il) Complexes: Structural and Electron Paramagnetic Resonance Studies of Substituent Steric Effects in an Extended Class of Pyrrolate-Imine Ligands', Journal of Coordination Chemistry, 56: 11, 975 — 993
To link to this Article: DOI: 10.1080/00958970310001607752
URL: http://dx.doi.org/10.1080/00958970310001607752

PLEASE SCROLL DOWN FOR ARTICLE

Full terms and conditions of use: http://www.informaworld.com/terms-and-conditions-of-access.pdf

This article may be used for research, teaching and private study purposes. Any substantial or systematic reproduction, re-distribution, re-selling, loan or sub-licensing, systematic supply or distribution in any form to anyone is expressly forbidden.

The publisher does not give any warranty express or implied or make any representation that the contents will be complete or accurate or up to date. The accuracy of any instructions, formulae and drug doses should be independently verified with primary sources. The publisher shall not be liable for any loss, actions, claims, proceedings, demand or costs or damages whatsoever or howsoever caused arising directly or indirectly in connection with or arising out of the use of this material.

J. Coord. Chem., Vol. 56, No. 11, 20 July 2003, pp. 975–993

Taylor & Francis
Taylor & Francis Group

FROM PLANAR TOWARD TETRAHEDRAL COPPER(II) COMPLEXES: STRUCTURAL AND ELECTRON PARAMAGNETIC RESONANCE STUDIES OF SUBSTITUENT STERIC EFFECTS IN AN EXTENDED CLASS OF PYRROLATE-IMINE LIGANDS

CHAMIKA M. WANSAPURA[a], CHOI JUYOUNG[a], JASON L. SIMPSON[a], DENNIS SZYMANSKI[b], GARETH R. EATON[b], SANDRA S. EATON[b] and STEPHEN FOX[a,*]

[a]*Department of Chemistry, University of Louisiana at Monroe, Monroe, LA 71209-0530, USA;* [b]*Department of Chemistry and Biochemistry, University of Denver, Denver, CO, USA*

(Received 26 November 2002; Revised 11 March 2003; In final form 22 April 2003)

Downloaded At: 13:44 23 January 2011

A series (**1a–1h**) of crystalline bis-pyrrolate-imine copper(II) complexes was isolated in good yield (typically 60–90%) by reaction of the Schiff base 2-*N*-(R)-pyrrolecarbaldimine (where R is an alkyl group of variable steric capacity) with a copper(II) salt and base in methanol or water. For new complexes **1f–1h**, pyrrolate-imine coordination is inferred by loss of ν(N–H) and a shift (ca. 40 cm^{-1}) to lower energy for ν(C=N) in the infrared spectra relative to free Schiff base. The X-ray crystal structures of **1f**, where R = benzyl, and **1g**, where R = diphenylmethyl, show trans geometry of the pyrrolate-imine moieties around Cu(II). The distortion from planarity of the CuN_4 coordination sphere, defined as the dihedral angle between the two chelating N(imine)–Cu–N(pyrrolate) planes, is 33.13(5)° for **1f** and 29.3° for **1g**. X-band electron paramagnetic resonance (EPR) spectra for **1a–1h** in glassy solutions (ca. 100 K) are approximately axial, with an inverse correlation between A_z and g_z. At room temperature in fluid solution there is an inverse correlation between A_{iso} and g_{iso}. Plots of A_z, A_{iso}, g_z, or g_{iso} as a function of the dihedral angles between the ligand planes in **1f** and **1g**, as well as the previously characterized **1a** (R = H) and **1d** (R = *tert*-butyl) were used to determine the dihedral angles of the four complexes of unknown geometry. A red-shift in the ligand field bands in the electronic absorption spectra in chloroform also correlates with increasing dihedral angle. For each of these correlations, the data point for the diphenylmethyl derivative **1g** deviates slightly from the line based on the other complexes; this is attributed to crystal packing forces causing a smaller dihedral angle for **1g** in the crystal than in solution.

Keywords: Copper(II) complex; Pyrrolate; Schiff base; Crystal structure; Dihedral angle; Electron paramagnetic resonance; Hyperfine

INTRODUCTION

The chemistry of monomeric copper(II) complexes is rich and continuously evolving, in part because of bioinorganic model studies, but also because of potential application to

*Author for correspondence. Tel.: (318) 342-1838. Fax: (318) 342-1859. E-mail: sfox@ulm.edu

ISSN 0095-8972 print: ISSN 1029-0389 online © 2003 Taylor & Francis Ltd
DOI: 10.1080/0095897031000160752

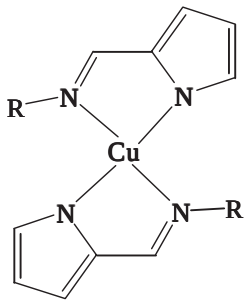

1a (R = H)
1b (R = methyl)
1c (R = *n*-butyl)
1d (R = *tert*-butyl)
1e (R = 1-adamantyl)
1f (R = benzyl)
1g (R = diphenylmethyl)
1h (R = 2-adamantyl)

FIGURE 1 General representation of bis-(pyrrolylcarbaldimine)copper(II).

Downloaded At: 13:44 23 January 2011

various catalytic processes, including oxidation catalysis. In our endeavors to generate complexes with potential catalytic activity, we are investigating chelating pyrrolate-imine ligands. Prior examples within this ligand class [1–3], lead us to predict that new derivatives will be robust and electron-rich, with π-bonding characteristics bestowed by the aromatic character of the pyrrole ring, and extending to the sp^2-hybridized imine nitrogen atom. Prior X-ray crystallographic characterizations [1,2] of Complexes **1a** and **1d** revealed trans bis-bidentate coordination as shown in Fig. 1.

The CuN_4 coordination sphere in bis-(*H*-pyrrolylcarbaldimine)copper(II), **1a** [1], is rigorously planar, whereas its *tert*-butyl analog **1d** is distorted toward tetrahedral geometry with a dihedral angle of ca. 61° between the two chelating N–Cu–N planes [2]. In spite of this difference in dihedral angle, the pyrrolate-imine moieties in both **1a** and **1d** remain essentially planar. It is generally accepted that distortion from planarity in the CuN_4 coordination center occurs as a result of steric interaction between the imine R group and the nearby pyrrolate ring of the other ligand.

Based on the essential congruence of mull and solution electronic absorption spectra of **1a**, and the invariance of solution spectra between chloroform and the potentially coordinating acetonitrile, it is reasonable to assume that the planar structure is retained in solution. The spectrum of **1a** in $CHCl_3$ displays two closely spaced bands of similar intensity ($\varepsilon \sim 200$) centered at 520 nm (19 200 cm^{-1}). In addition, a number of alkyl-substituted analogs (R = *n*-butyl, isopropyl, methyl, and *sec*-butyl) have been studied [4,5,6] with congruence of the solution and mull spectra again observed. All these compounds exhibit a fairly intense peak ($\varepsilon \sim 1100$–1200) around 400–425 nm (25 000 to 23 500 cm^{-1}), which is considered to result from a ligand-centered transition [4]. By virtue of the common features of a band around 520 nm, ascribed to a ligand-field transition, with a low energy shoulder appearing as a result of the distortion away from C_{2h} point symmetry, Complexes **1a–lc**, and **1e** are considered to have similar structures, with varying degrees of distortion from planarity [6]. In contrast, **1d** exhibits a ligand-field transition at 645 nm (15 500 cm^{-1}), at least 100 nm lower in energy, resulting from the major distortion toward tetrahedral geometry [5,6].

Yokoi and Addison [6] studied the visible absorption and electron paramagnetic resonance (EPR) spectra of a large series of pyrrolate-imine complexes of copper(II), including **1a–1e**, and found an inverse correlation between A_z and g_z as well as between the higher and lower energy ligand-field transition energies, ΔE, and g_z. Moreover, using the dihedral angle values for **1a** and **1d**, as well as those from related structures [7,8], it was found that g_z increased with increasing dihedral angle, and that

the dependence on dihedral angle was stronger for complexes with a dihedral angle $>60^\circ$ than for complexes with a smaller dihedral angle [6].

Other four-coordinate copper(II) complexes have also been studied, some with CuN_2S_2 coordination. Bereman and co-authors [9] prepared three 2-amino-1-cyclopentenedithiocarboxylato complexes with a variable linker unit between the chelating halves of the molecules to strategically induce tetrahedral distortion, and thereby model the coordination geometry of Type I copper proteins. For two members of the series, dihedral angles of 52.8° and 57.1° were established from structural determinations. A red-shift of the lowest energy ligand-field peak in the electronic spectrum occurred for increasing distortion. The inverse correlation between these dihedral angles and A_z values observed from EPR spectra measured at 100 K could be extrapolated to fit well with the A_z values of several Type I copper proteins, and therefore predict the dihedral angles in those proteins.

To more fully define the relationship between geometry and EPR and visible spectral properties of copper(II) pyrrolate-amine complexes, we have prepared and studied **1f**–**1h**, in addition to the previously characterized complexes **1a**–**1e**. X-ray crystal structures were determined for **1f** and **1g**, which, in combination with the literature data for **1a** and **1d**, provide four different dihedral angles within the range of 0–61°.

Downloaded At: 13:44 23 January 2011

EXPERIMENTAL

Materials and Routine Physical Measurements

Pyrrole-2-carbaldehyde and copper tetrafluoroborate hydrate were purchased from Aldrich Chemical Company. Amines used in the Schiff-base formation were purchased from Aldrich Chemical Company except benzylamine, which was purchased from Acros Company. Solvents were reagent grade and were used without further purification. Melting points were recorded using an electrothermal EM-6 apparatus, and were not corrected. Nuclear magnetic resonance spectra were recorded using a Jeol Eclipse 300 MHz spectrometer. Infrared spectra were recorded as Nujol mulls between NaCl plates on a Perkin-Elmer Paragon FTIR spectrometer. Electronic absorption spectra were recorded using a Shimadzu UV-1601 scanning spectrophotometer. Mass spectrometry measurements were recorded using the electron impact (70 eV) technique on a Finnigan Mat GCQ instrument. Elemental analysis was performed by Desert Analytics of Tucson, Arizona.

EPR Spectroscopy

EPR spectra were obtained on a Varian E9 X-band (9.22 GHz) spectrometer equipped with a TE_{102} resonator and liquid nitrogen gas-flow system. Samples were ca. 1 mM in 2 : 1 toluene : chloroform. Enough solution was transferred to a 4-mm O.D. EPR sample tube, to fill to about 1 in. For fluid solutions, spectra were recorded with a center field of 3150 G and a sweep width of 1000 G. For each sample the spectra were checked for power saturation. The signal amplitude increased linearly with $\sqrt{P}$ between 20 and 80 mW. The spectra were run at 50 mW, with a modulation amplitude of 4 G and a time constant of 0.128 s. For glassy solutions at ca. 100 K, spectra were

recorded with a center field of 3050 G, a sweep width of 1000 G, microwave powers between 0.1 and 4.0 mW, and a modulation amplitude of 4 G.

Fluid solution spectra were simulated with the locally written program, Asym, which includes both copper nuclear isotopes, linewidths that depend on nuclear hyperfine spin, and second-order corrections to the transition energies [10]. The values of g_{iso}, A_{iso}, and linewidths were manually adjusted to match the spectra. Low-temperature spectra were simulated with the locally written program, Monmer, which is based on classical equations [11]. The values of g_z and A_z could be defined relatively well. Values of g_x, g_y, A_x, and A_y were not well defined because multiple features contribute to the same region of the spectrum. Spectra at more than one microwave frequency would be required to adequately define those parameters. The estimated uncertainties were A_{iso}, $\pm 1.5 \times 10^{-4}\,cm^{-1}$; g_{iso}, ± 0.003; A_z, $\pm 2.5 \times 10^{-4}\,cm^{-1}$; and g_z, ± 0.002.

For the complexes for which X-ray crystal structures are known (**1a**, **1d**, **1f**, **1g**) values of g_{iso}, A_{iso}, g_z, or A_z were plotted as a function of dihedral angle and a line was drawn through the points. For the remaining complexes (**1b**, **1c**, **1e**, **1h**) the dihedral angle was estimated by reading from each plot the angle that corresponded to the observed value of g_{iso}, A_{iso}, g_z, or A_z. The ranges of angles estimated from the plots of the four parameters were **1b**, 13–16°; **1c**, 25–29°; **1h**, 35–37°; **1e**, 60–61°.

Downloaded At: 13:44 23 January 2011

X-ray Crystallography

A dark-red block crystal of **1f** (of approximate dimensions $0.40 \times 0.30 \times 0.10\,mm^3$) and a black block crystal of **1g** (of approximate dimensions $0.25 \times 0.25 \times 0.20\,mm^3$) were placed on the tips of 0.1-mm diameter glass capillaries and mounted on a Siemens SMART system for data collections at 173(2) K using graphite-monochromated Mo Kα radiation (0.71703 Å). In each case, the intensity data were corrected for Lorentz polarization effects and absorption [12,13]. The space group $P2_1/n$ was determined for **1g** based on systematic absences and intensity statistics. Final cell constants were calculated from 3399 strong reflections for **1f**, and from 3785 strong reflections for **1g**. Other details of crystal data, data collection and processing are given in Tables I and II.

The structures were solved by direct methods: use of SHELXS-97 [14] for **1f** and SHELXS-86 [14] for **1g** provided most of the non-hydrogen atoms. Full-matrix least-squares/difference Fourier cycles were performed using SHELXL-97 [14] in order to locate the remaining non-hydrogen atoms. All non-hydrogen atoms were refined with anisotropic displacement parameters. All hydrogen atoms were placed in ideal positions and refined as riding atoms with isotropic displacement parameters related to the parent atom.

Preparation of the Schiff Bases

2-N-(1-benzyl)pyrrolecarbaldimine The Schiff base 2-*N*-(benzyl)pyrrolecarbaldimine was prepared differently from the literature method [5] by combining equimolar amounts (20.0 mmol) of benzylamine with pyrrole-2-carbaldehyde in ethanol (20 mL) at 25°C; upon stirring for 4 h, the product crystallized directly from solution as white needles, which were collected by filtration, washed with ethanol (5 mL) and allowed to air-dry (yield 18.0 mmol, 90%). Mp: 101–102°C. ^{1}H-NMR ($CDCl_3$, δ): 4.75 (s, 2H, N–C*H*$_2$), 6.22 (t, 1H, pyrr–*H*), 6.55 (dd, 1H, pyrr–*H*), 6.68 (s, 1H, pyrr–*H*), 7.35–7.30

TABLE I Crystal data and structure refinement details for **1f**

Empirical formula	$C_{24}H_{22}CuN_4$
Formula weight	430.00
Crystal system	Triclinic
Space group	*P*-1
Unit cell dimensions	$a = 8.7336(6)$ Å $\alpha = 91.431(1)^\circ$ $b = 10.7231(8)$ Å $\beta = 104.732(1)^\circ$ $c = 11.3634(8)$ Å $\gamma = 91.776(1)^\circ$
Volume	1028.12(13) Å^3
Z	2
Density (calculated)	1.389 Mg/m^3
Absorption coefficient	1.079 mm^{-1}
F(000)	446
Index ranges	$-10 = h = 10$, $-13 = k = 13$, $-14 = l = 14$
Reflections collected	8564
Independent reflections	4158 [R(int) = 0.016]
Observed reflections	3767
Completeness to $\theta = 26.41^\circ$	98.7%
Absorption correction	Semi-empirical from equivalents
Max. and min. transmission	0.900 and 0.752
Refined parameters	262
Goodness-of-fit on F^2	1.092
Final R indices [$I > 2$sigma(I)]	$R1 = 0.0301$, $wR2 = 0.0858$
R indices (all data)	$R1 = 0.0334$, $wR2 = 0.0879$
Largest difference peak and hole	0.601 and -0.297 e Å^{-3}

Downloaded At: 13:44 23 January 2011

TABLE II Crystal data and structure refinement for **1g**

Empirical formula	$C_{36}H_{30}CuN_4$
Formula weight	582.18
Temperature	173(2) K
Wavelength	0.71073 Å
Crystal system	Monoclinic
Space group	$P2_1/n$
Unit cell dimensions	$a = 16.730(3)$ Å $\alpha = 90^\circ$ $b = 9.8635(17)$ Å $\beta = 106.734(3)^\circ$ $c = 17.878(3)$ Å $\gamma = 90^\circ$
Volume	2825.2(8) Å3
Z	4
Density (calculated)	1.369 Mg/m3
Absorption coefficient	0.806 mm^{-1}
F(000)	1212
Crystal color and habit	Black, block
Crystal size	$0.25 \times 0.25 \times 0.20$ mm^3
θ range for data collection	1.47 to 27.97°
Index ranges	$-22 \le h \le 21$, $0 \le k \le 13$, $0 \le l \le 23$
Reflections collected	34448
Independent reflections	6772 [R(int) = 0.0447]
Observed reflections	5551
Completeness to $\theta = 27.97^\circ$	99.8%
Absorption correction	Multiscan
Max. and min. transmission	0.8555 and 0.8240
Refinement method	Full-matrix least-squares on F^2
Data/restraints/parameters	6772/0/370
Goodness-of-fit on F^2	1.058
Final R indices [$I > 2\sigma$(I)]	$R1 = 0.0359$, $wR2 = 0.0908$
R indices (all data)	$R1 = 0.0488$, $wR2 = 0.0981$
Largest diff. peak and hole	0.730 and -0.317 e Å^{-3}

(m, 5H, Ar–*H*), 8.19 (s, 1H, –C*H*=N). IR (Nujol, ν, cm^{-1}): 3166 (N–H), 2888, 1635 (C=N), 1452, 1422, 1377, 1358, 1305, 1132, 1096, 1028, 985, 974, 946, 907, 787, 734, 698, 603. MS: (70 eV, electron impact) m/z 185 (M + 1), 184, 168.

2-N-(1-adamantyl)pyrrolecarbaldimine In a 250-mL Erlenmeyer flask equipped with stir bar was dissolved pyrrole-2-carbaldehyde (1.90 g; 20.0 mmol) in ethanol (20 mL). To this stirred solution was introduced 1-adamantanamine (3.02 g, 20.0 mmol) as a white solid, which dissolved freely. After 6 h, a cake of white product had formed to which water was added (100 mL). The ensuing mixture was suction-filtered to collect a white solid which was washed with water, and allowed to air-dry to yield a white powder (3.82 g, 84%) suitable for complexation reactions. Mp 155–156°C. IR (Nujol, ν, cm^{-1}): 3126 (N–H), 2956, 1636 (C=N), 1457, 1376, 1307, 1154, 1086, 1040, 983, 965, 917, 882, 775, 732, 615. ^{1}H-NMR ($CDCl_3$, δ): 1.68 (s, 6H, CH_2), 1.75 (s, 6H, CH_2), 2.14 (s, 3H, C*H*), 6.21 (t, 1H, pyrr–*H*), 6.45 (dd, 1H, pyrr–*H*), 6.83 (s, 1H, pyrr–*H*), 8.10 (s, 1H, –C*H*=N), 8.60 (br s, N–H). MS: (70 eV, electron impact) m/z 228 (molecular ion), 227 (M − 1), 171.

2-N-(2-adamantyl)pyrrolecarbaldimine In a 250-mL Erlenmeyer flask equipped with stir bar was introduced 2-adamantanamine hydrochloride (3.80 g, 20.0 mmol), as a white solid, and ethanol (20 mL). To this stirred suspension was added triethylamine (2.02 g, 20.0 mmol) to effect dissolution. Pyrrole-2-carbaldehyde (1.90 g, 20.0 mmol) was then added as a solid, and quickly dissolved to yield a pale-yellow solution, which was stirred vigorously. After 4 h, a cake of ecru product had formed to which was added water (150 mL); stirring of the ensuing suspension was continued for 2 h. The product was collected by suction filtration, washed with water (50 mL), and allowed to air-dry to yield a cream powder (2.89 g, 63%) suitable for complexation reactions. Mp 91–92°. IR (Nujol, ν, cm^{-1}): 3126 (N–H), 2925, 1636 (C=N), 1460, 1377, 1136, 1098, 1080, 1052, 1027, 936, 882, 727, 607. ^{1}H-NMR ($CDCl_3$, δ): 1.53 (d, 2H, CH_2), 1.70–1.90 (m, 10H, C*H*), 2.31 (d, 2H, –C*H*–), 3.42 (s, 1H, –C*H*–N), 6.23 (t, 1H, pyrr–*H*), 6.49 (dd, 1H, pyrr–*H*), 6.90 (s, 1H, pyrr–*H*), 8.10 (br s, N–H), 8.10 (s, 1H, –C*H*=N). MS: (70 eV, electron impact) m/z 227 (M − 1), 212.

2-N-(1-diphenylmethyl)pyrrolecarbaldimine In a 250-mL Erlenmeyer flask equipped with stir bar was dissolved pyrrole-2-carbaldehyde (1.90 g, 20.0 mmol) in ethanol (20 mL). To this solution was introduced aminodiphenylmethane (3.665 g, 20.00 mmol) to form a pale-yellow solution, which was stirred vigorously. After 6 h, a sticky mass had formed to which was added water (100 mL) to precipitate a copious white oil, which solidified over the next 48 h. The ensuing mixture was suction-filtered to collect a crumbly off-white solid, which was washed with water, and allowed to air-dry to yield a cream powder (4.210 g, 81%) suitable for complexation reactions. Mp: 71–72°C. ^{1}H-NMR ($CDCl_3$, δ): 5.23 (br s, N–H), 5.56 (s, 1H, N–C*H*), 6.22 (t, 1H, pyrr–*H*), 6.51 (dd, 1H, pyrr–*H*), 6.78 (s, 1H, pyrr–*H*), 7.36–7.26 (m, 10H, Ar–*H*), 8.20 (s, 1H, –C*H*=N). IR (Nujol, ν, cm^{-1}): 3166 (N–H), 2924, 1634 (C=N), 1492, 1461, 1421, 1377, 1313, 1132, 1094, 1034, 884, 782, 756, 742, 729, 698, 604. MS: (70 eV, electron impact) m/z 260 (molecular ion), 167.

Preparation of the Complexes

Complexes **1a**–**1d** were prepared according to the following general procedure: in a 250-mL Erlenmeyer flask was dissolved pyrrole-2-carbaldehyde (0.930 g, 10.0 mmol)

Downloaded At: 13:44 23 January 2011

in water (30 mL) and the contents warmed to ca. 60°C. To this solution was added another prepared from copper(II) sulfate pentahydrate (2.50 g, 10.0 mmol) dissolved in a 10% aqueous solution of the relevant amine (20 mL). The ensuing blue solution was allowed to stand for ca. 10 min. A solution of sodium hydroxide (0.400 g, ~10.0 mmol) in water (30 mL) was then added dropwise with occasional swirling to produce a sparkling precipitate. The ensuing suspension was allowed to stand for 1 h, whereupon it was suction-filtered to collect a microcrystalline dark solid, which was washed with water (10 mL), and allowed to air-dry. Recrystallization from hot methanol yielded red-brown plates of **1a**; recrystallization from hot heptane yielded dark needles of **1b**, and dark blocks of **1c**; and recrystallization from hot hexanes yielded dark green blocks of **1d**. All compounds gave satisfactory elemental analyses and matched literature characterization by melting point, and electronic absorption spectra.

*Bis(2-N-1-adamantyl-pyrrolylcarbaldimine)copper(II), (**1e**)* This known complex [6] was prepared by the following novel route: to a solution of 2-*N*-(1-adamantyl)pyrrolecarbaldimine (2.28 g, 10.0 mmol) in methanol (40 mL) was added $Cu(BF_4)_2 \cdot xH_2O$ (19–22% Cu by weight) (1.58 g, 5.0 mmol) and triethylamine (1.01 g, 10.0 mmol). The ensuing green suspension was stirred for 15 min; the product was collected by suction-filtration, washed with methanol (10 mL), and air-dried to yield a green microcrystalline solid (2.10 g, 81%). Recrystallization was effected from hot hexanes. Mp 198–199°. Anal. Calcd for $C_{30}H_{38}N_4Cu$: C, 69.53; H, 7.39; N, 10.81; Cu, 12.26. Found: C, 69.88; H, 7.70; N, 10.75; Cu, 11.76. IR (Nujol, ν, cm^{-1}): 2922, 1583 (C=N), 1455, 1377, 1319, 1301, 1260, 1197, 1186, 1111, 1088, 1032, 994, 982, 929, 896, 822, 744, 730, 674, 619. UV-vis: ($CHCl_3$; λ_{max}, nm (ε, $M^{-1}\,cm^{-1}$)): 423 nm (1210), 641 nm (250).

*Bis(2-N-benzyl-pyrrolylcarbaldimine)copper(II), (**1f**)* The dissolution of 2-*N*-(benzyl)pyrrolecarbaldimine (0.575 g, 3.10 mmol) in methanol (30 mL) was followed by addition of $Cu(BF_4)_2 \cdot xH_2O$ (19–22% Cu by weight) (0.500 g, 1.50 mmol) and triethylamine (0.303 g, 3.00 mmol). The ensuing dark-green solution was left to stand for 15 h; the product was collected by suction-filtration, washed with methanol (10 mL), and air-dried to yield sparkling black needles (0.363 g, 56%). Recrystallization from acetonitrile yielded dark plates. Mp 118–120°. Anal. Calcd for $C_{24}H_{22}N_4Cu$: C, 67.04; H, 5.16; N, 13.03; Cu, 14.78. Found: C, 67.13; H, 5.45; N, 13.03; Cu, 14.55. IR (Nujol, ν, cm^{-1}): 2924, 1596 (C=N), 1463, 1377, 1347, 1319, 1225, 1198, 1082, 1067, 1036, 976, 958, 895, 860, 842, 810, 741, 694, 608. UV-vis: ($CHCl_3$; λ_{max}, nm (ε, $M^{-1}\,cm^{-1}$)): 421 nm (1210), 529 nm (240), 683 nm (sh, 140).

*Bis(2-N-diphenylmethylpyrrolylcarbaldimine)copper(II), (**1g**)* The dissolution of 2-*N*-(1-diphenylmethyl)pyrrolecarbaldimine (0.520 g, 2.00 mmol) in methanol (20 mL) was followed by addition of $Cu(BF_4)_2 \cdot xH_2O$ (19–22% Cu by weight) (0.330 g, 1.00 mmol) and triethylamine (0.202 g, 2.00 mmol). The ensuing green-brown solution was left to stand for 15 min; the product was collected by suction-filtration, washed with methanol (10 mL), and air-dried to yield sparkling brown microcrystals (0.356 g, 61%). Recrystallization from hot acetonitrile yielded black blocks. Mp 188–191°. Anal. Calcd for $C_{36}H_{30}N_4Cu$: C, 74.27; H, 5.19; N, 9.62; Cu, 10.91. Found: C, 73.97; H, 5.65; N, 9.72; Cu, 11.20. IR (Nujol, ν, cm^{-1}): 2886, 1590 (C=N), 1463, 1377, 1309, 1244, 1171, 1078, 1032, 1016, 927, 896, 812, 765, 741, 700, 668, 609. UV-Vis: ($CHCl_3$; λ_{max}, nm (ε, $M^{-1}\,cm^{-1}$)): 423 nm (970), 549 nm (230), 698 nm (sh, 140).

Downloaded At: 13:44 23 January 2011

*Bis(2-N-2-adamantyl-pyrrolylcarbaldimine)copper(II), (**1h**)* The dissolution of 2-*N*-(2-adamantyl)pyrrolecarbaldimine (1.14 g, 5.0 mmol) in methanol (40 mL) was followed by addition of $Cu(BF_4)_2 \cdot xH_2O$ (19–22% Cu by weight) (0.79 g, 2.5 mmol) and triethylamine (0.505 g, 5.0 mmol). The ensuing pale-green suspension was allowed to stand for 15 min, whereupon a copious precipitate formed; the product was collected by suction-filtration, washed with methanol (20 mL), and air-dried to yield a light-green powder (1.10 g, 85%). Recrystallization as dark-brown needles was effected from hot acetonitrile solution. Mp 199–200°. Anal. Calcd for $C_{30}H_{38}N_4Cu$: C, 69.53; H, 7.39; N, 10.81; Cu, 12.26. Found: C, 69.59; H, 7.53; N, 10.84; Cu, 12.27. IR (Nujol, ν, cm^{-1}): 2922, 1597 (C=N), 1455, 1377, 1323, 1296, 1261, 1220, 1199, 1178, 1102, 1083, 1058, 1030, 994, 966, 941, 896, 858, 830, 816, 730, 674, 634, 610. UV-Vis: ($CHCl_3$; λ_{max}, nm (ε, $M^{-1}\,cm^{-1}$)): 419 nm (1160), 553 nm (300), 708 nm (sh, 170).

RESULTS

The melting point and signature ^{1}H-NMR features of the benzyl-substituted Schiff base (N=C–H resonance, CH_2 resonances, pyrrole and benzene ring resonances) are all consistent with a literature report [15]. The novel Schiff-base analogs with R = 1-adamantyl, 2-adamantyl, and diphenylmethyl all gave sharp melting points and clean NMR spectra with a C–H (imine) proton in the range of 8.10 to 8.20 δ, three distinct pyrrole protons in the range 6.20 to 6.90 δ, and other expected signals to account for the various R groups. The four Schiff bases isolated also demonstrated strong absorptions in the range 1630–1640 cm^{-1} consistent with ν(C=N), as well as observed ν(N–H) around 3200 cm^{-1}. The GC/MS spectra for these four compounds showed the molecular ion peak or M-1 peak in all cases.

Complexation was effected through (a) introduction of Schiff bases, $Cu(BF_4)_2$ and stoichiometric triethylamine in methanol to form **1e**–**1h**, and (b) introduction of amine, copper(II) sulfate, pyrrole-2-carbaldehyde and stoichiometric sodium hydroxide in water to form **1a**–**1d** [16]. All complexes precipitated from the green to brown reaction solutions as dark crystalline solids, and were recrystallized from CH_3OH, CH_3CN, heptane, or hexanes. Prolonged standing in solution in acetone or tetrahydrofuran resulted in substantial decomposition. Attempts to prepare the extremely sterically hindered R = triphenylmethyl (trityl) complex, or its Schiff base, by either method used in this report yielded only starting material.

The infrared spectra of all complexes show loss of the pyrrole ν(N–H) and a pronounced shift in ν(C=N) to 1570–1595 cm^{-1} (Table III). For **1a**, the anticipated imine ν(N–H) appeared at 3320 cm^{-1}. All complexes except **1a** were found to melt quite sharply in the range 90–200°C, and with melting points consistent with literature values where relevant. The complex **1a** did not melt up to 410°C, but appeared to darken and decompose to a dark solid at ca. 150°C. All complexes dissolved readily in chloroform and remained in solution in the 2 : 1 toluene–chloroform mixtures used for EPR measurements. All eight complexes gave elemental analyses for C, H, N, and Cu consistent with high purity as appropriate for the ensuing EPR studies.

The electronic absorption spectra of complexes **1a**–**1e** in chloroform matched those reported previously [4–6]. The eight complexes studied are listed in Table I in order of decreasing energies of the ligand-field transitions in chloroform solution. For benzyl derivative **1f**, the spectrum is very similar in profile and intensity to that of

Downloaded At: 13:44 23 January 2011

TABLE III Ligand-field transitions and imine vibrations for **1a-h**[a]

R-group (*identifier*)	*Vis* (λ_{max}, cm^{-1} (ε, $M^{-1}cm^{-1}$))		$\nu(C{=}N)$ (cm^{-1})
R = H (**1a**)	19 800 (210)	18 700 (210)	1574
R = methyl (**1b**)	19 500 (270)	14 900 (120)	1592
R = *n*-butyl (**1c**)	19 000 (240)	14 700 (145)	1594
R = benzyl (**1f**)	18 900 (240)	14 600 (140)	1596
R = diphenylmethyl (**1g**)	18 200 (230)	14 300 (140)	1590
R = 2-adamantyl (**1h**)	18 100 (300)	14 100 (170)	1597
R = *tert*-butyl (**1d**)	15 600 (250)		1591
R = 1-adamantyl (**1e**)	15 600 (250)		1583

[a]Electronic spectra were obtained in $CHCl_3$ solution. IR spectra were obtained as nujol mulls. Compounds are listed in order of decreasing energy for the ligand-field transitions.

1c, the *n*-butyl derivative, except for a very slight red-shift for each peak. The higher energy d–d transition for the diphenylmethyl analog **1g**, however, is red-shifted to 18 200 cm^{-1}, compared to 18 900 cm^{-1} in **1f**. The ligand-field region for the 2-adamantyl counterpart, **1h**, is very slightly red-shifted from **1g**. The spectra of all complexes dissolved in acetonitrile are essentially unchanged from those in chloroform.

The structure of **1f** was solved in the space group *P*-1, where the necessary crystallographic inversion center lies between the molecules comprising the unit cell; this symmetry element is readily envisioned in the packing diagram (Fig. 2). A complete list of crystal data and structure refinement parameters appears in Table I. The atom numbering scheme for **1f** is shown on the ORTEP diagram (Fig. 3), and important bond distances and angles in **1f** are found in Table IV. The structure of **1g** was solved in the space group $P2_1/n$; the atom numbering scheme is shown on the ORTEP diagram (Fig. 4), and important bond distances and angles in **1g** are found in Table V.

Downloaded At: 13:44 23 January 2011

Inspection of the pertinent torsion angles within the chelating region of each ligand in **1f** and **1g** reveals that N–C–C=N, in addition to the entire pyrrolate ring, can be considered as a planar unit. The relevant averaged intraligand distances for **1f** and **1g** are reported and compared with **1a** and **1d** in Table VI; specific angles and distances are found in Tables IV and V. Furthermore, from the packing diagrams (Figs. 2 and 4), the phenyl groups of the substituents within both **1f** and **1g** appear rotated away from the pyrrolate rings of the second ligand of the same molecule, in order to minimize intramolecular contacts, and to facilitate "stacking" with analogous phenyl groups in neighboring molecules. It also appears that pyrrolate-imine groups are parallel to analogs in neighboring molecules.

The defining features of both structures are the (imine)N–Cu–N(imine) angle, which is 149.06(6)° in **1f**, and 161.98(6)° in **1g**, and the (pyrrolate)N–Cu–N(pyrrolate) angle which is almost linear at 172.48(6)° for **1f**, and less open at 159.48(6)° in **1g**. Consequently, there is a dihedral angle of 33.13(5)° between the two "coordination" planes N7–Cu1–N1 and N27–Cu1–N21 in **1f**, and a corresponding angle of 29.3° between N1–Cu1–N2 and N3–Cu1–N4 in **1g**. There do not appear to be any significantly short intermolecular contacts such as between non-bonding hydrogen atoms, or axial contacts to the metal, in either structure. Intermolecular contacts of possible interest for **1f** are, H6a···H8a = 2.205 Å and H8a···H22a = 2.30 Å (the closest contact across the molecule, between the chelates); for **1g**, the analogous contacts are: H5a···H12a = 2.96 Å and H6a···H19a = 2.18 Å.

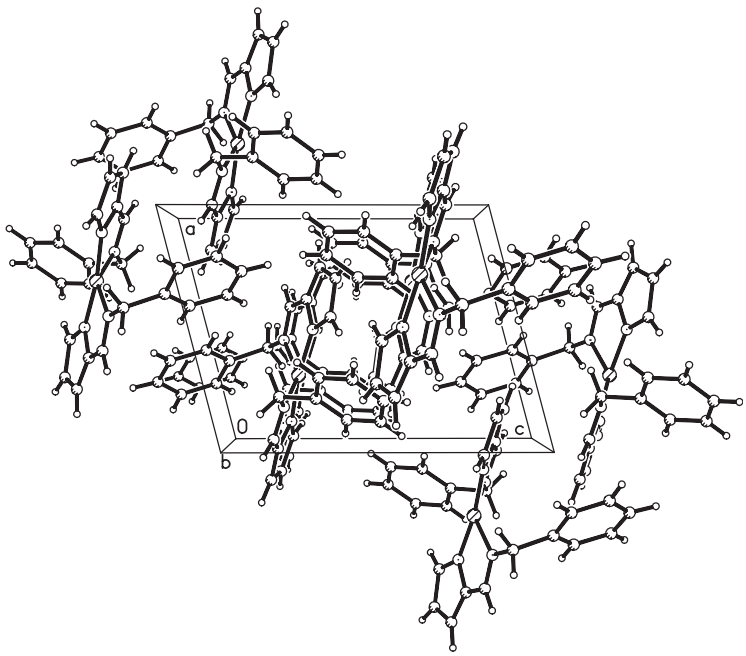

FIGURE 2 Packing diagram for complex **1f**.

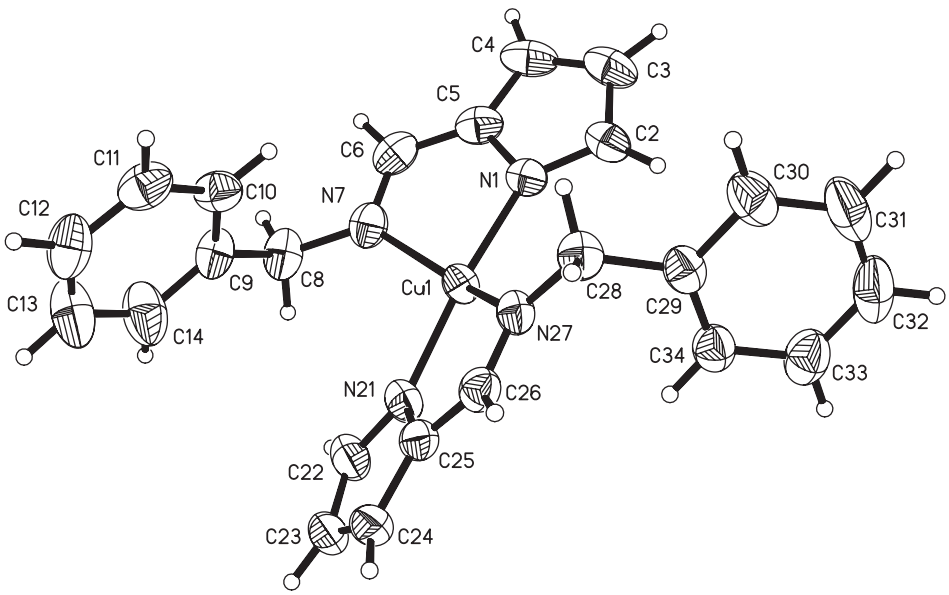

FIGURE 3 Structure of **1f** showing atom numbering scheme.

Examples of the range of EPR spectra that were observed in fluid solution are shown in Fig. 6. The copper hyperfine splitting decreased in the order **1a** > **1b** > **1h** > **1e**, which is also the order of decreasing energies of the ligand-field transitions (Table III). Values of g_{iso} increased as A_{iso} decreased (Table VII). Although hyperfine splitting from the

Downloaded At: 13:44 23 January 2011

TABLE IV Selected metric parameters (Å and °) for **1f**

Cu1–N1	1.9539(15)	C6–N7	1.293(3)
Cu1–N21	1.9641(16)	N7–C8	1.456(3)
Cu1–N7	2.0380(16)	N21–C22	1.354(2)
Cu1–N27	2.0383(15)	N21–C25	1.368(3)
N1–C2	1.346(2)	C22–C23	1.391(3)
N1–C5	1.378(3)	C23–C24	1.390(3)
C2–C3	1.399(3)	C24–C25	1.394(3)
C3–C4	1.390(4)	C25–C26	1.422(3)
C4–C5	1.392(3)	C26–N27	1.288(2)
C5–C6	1.420(3)	N27–C28	1.454(2)
N1–Cu1–N21	172.48(6)	N7–Cu1–N1/N27–Cu1–N21	33.13(5)
N1–Cu1–N7	82.76(7)		
N21–Cu1–N7	99.49(7)		
N1–Cu1–N27	99.32(6)		
N21–Cu1–N27	82.48(6)		
N7–Cu1–N27	149.06(6)		
C2–N1–C5	106.64(16)		
C2–N1–Cu1	141.11(14)		
C5–N1–Cu1	111.80(13)		
N1–C2–C3	110.4(2)		
C4–C3–C2	106.68(19)		
C3–C4–C5	106.41(19)		
N1–C5–C4	109.90(19)		
N1–C5–C6	115.94(17)		
C4–C5–C6	134.1(2)		
N7–C6–C5	118.40(18)		
C6–N7–C8	119.42(17)		
C6–N7–Cu1	111.05(14)		
C8–N7–Cu1	129.51(14)		
N7–C8–C9	113.67(16)		
C10–C9–C14	118.54(19)		
C10–C9–C8	121.37(19)		
C14–C9–C8	120.09(19)		
C22–N21–C25	106.14(17)		
C22–N21–Cu1	142.37(15)		
C25–N21–Cu1	111.36(12)		
N21–C22–C23	110.6(2)		
C24–C23–C22	106.79(18)		
C23–C24–C25	105.98(19)		
N21–C25–C24	110.50(18)		
N21–C25–C26	116.48(16)		
C24–C25–C26	133.01(19)		
N27–C26–C25	118.06(17)		
C26–N27–C28	118.49(16)		
C26–N27–Cu1	111.08(13)		
C28–N27–Cu1	129.95(13)		
N27–C28–C29	113.76(15)		

Downloaded At: 13:44 23 January 2011

ligand nitrogens was partially resolved only in the spectra of **1h**, lineshape simulations required nitrogen hyperfine splittings in all of the spectra, with values that decreased from $14 \times 10^{-4}\,cm^{-1}$ for **1a** to $10 \times 10^{-4}\,cm^{-1}$ for **1d** and **1e**. Distinctions between the two types of nitrogen donors were too small to detect. Typical rigid lattice spectra are shown in Fig. 7. The value of A_z decreased and g_z increased in the order **1a** > **1b** > **1h** > **1e**, which parallels the trends observed in fluid solution. Computer simulations of the lineshapes showed that the hyperfine splitting from ligand nitrogens decreased from $15 \times 10^{-4}\,cm^{-1}$ for **1a** to $9 \times 10^{-4}\,cm^{-1}$ for **1d** and **1e**. The EPR spectral

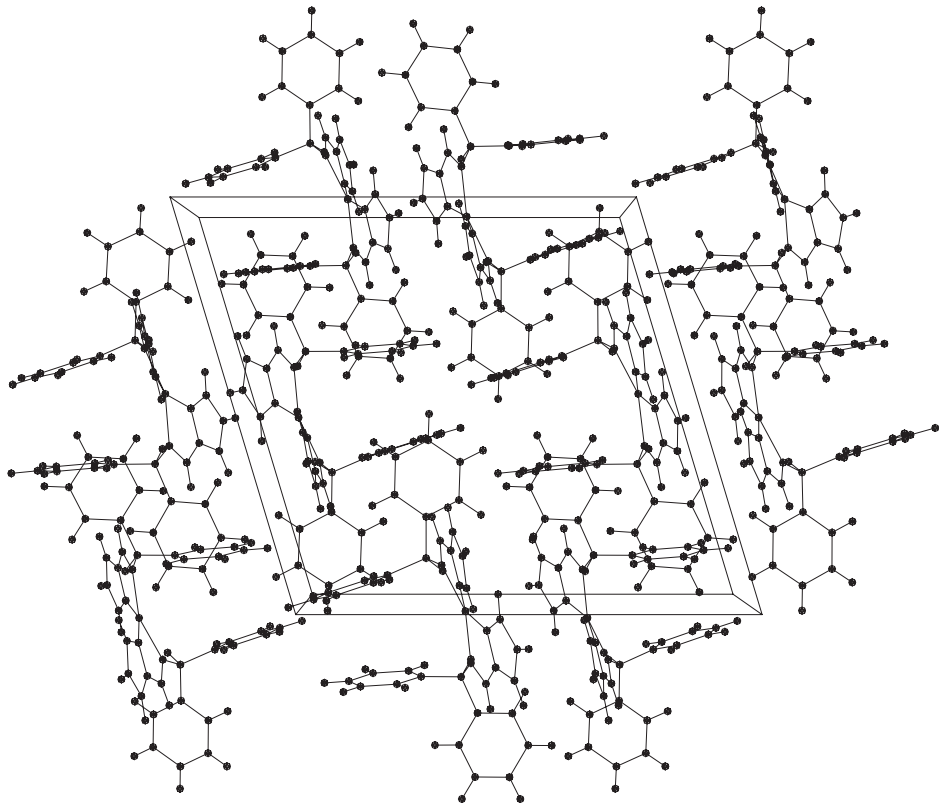

FIGURE 4 Packing diagram for complex **1g**.

Downloaded At: 13:44 23 January 2011

parameters g_{iso}, A_{iso}, g_z, and A_z for the eight complexes are listed in Table VII in the same order as in Table III. The trends in the EPR parameters correlate with the trends in the electronic transitions, consistent with a dependence on coordination geometry. The EPR parameters for **1a–1e** are in reasonable agreement with the literature [6]. Fluid solution g_{iso} and A_{iso} values agree within experimental uncertainty. The rigid lattice A_z values are smaller by up to about 5% than reported for toluene solutions [6] and g_z values are small by up to 0.008, which is attributed to the change in solvent and the fact that the present values were obtained by computer simulation, including second-order corrections. The benzyl derivative **1f** shows remarkable similarity in all values to the *n*-butyl analog, **1c**, and resembles somewhat the other new Complexes **1g** and **1h**.

DISCUSSION

The syntheses of three new copper(II) complexes of pyrrolate-imine ligands, **1f–1h**, are reported here. No infrared spectra of the known **1a–1e** were cited in earlier reports [1,2,3,6]. The shift observed here to lower energy for ν(C=N) in **1e–1h** upon complexation of the Schiff base ($40\,cm^{-1}$), is not unusual. For example, the dimeric bis-bidentate [*N*,*N*′-di-(2-pyrrolylmethylenyl-1,2-ethanediamine]copper(II) complex [3,17]

TABLE V Selected metric parameters (Å and °) for **1g**

Cu1–N3	1.9442(15)	C17–H17A	0.9500
Cu1–N1	1.9691(15)	C18–H18A	0.9500
Cu1–N4	2.0183(15)	N3–C19	1.348(2)
Cu1–N2	2.0313(15)	N3–C22	1.370(2)
N1–C1	1.349(2)	C19–C20	1.393(3)
N1–C4	1.367(2)	C19–H19A	0.9500
C1–C2	1.390(3)	C20–C21	1.392(3)
C1–H1A	0.9500	C20–H20A	0.9500
C2–C3	1.391(3)	C21–C22	1.392(3)
C2–H2A	0.9500	C21–H21A	0.9500
C3–C4	1.390(3)	C22–C23	1.413(3)
C3–H3A	0.9500	C23–N4	1.291(2)
C4–C5	1.414(3)	C23–H23A	0.9500
C5–N2	1.293(2)	N4–C24	1.468(2)
C5–H5A	0.9500	C24–C31	1.513(3)
N2–C6	1.476(2)	C24–C25	1.522(2)
C6–C13	1.523(3)	C24–H24A	1.0000
C6–C7	1.524(2)	C25–C26	1.384(3)
C6–H6A	1.0000	C25–C30	1.392(3)
C7–C12	1.389(3)	C26–C27	1.388(3)
C7–C8	1.390(3)	C26–H26A	0.9500
C8–C9	1.384(3)	C27–C28	1.375(3)
C8–H8A	0.9500	C27–H27A	0.9500
C9–C10	1.384(3)	C28–C29	1.388(3)
C9–H9A	0.9500	C28–H28A	0.9500
C10–C11	1.378(3)	C29–C30	1.386(3)
C10–H10A	0.9500	C29–H29A	0.9500
C11–C12	1.385(3)	C30–H30A	0.9500
C11–H11A	0.9500	C31–C32	1.381(3)
C12–H12A	0.9500	C31–C36	1.387(3)
C13–C18	1.386(3)	C32–C33	1.388(3)
C13–C14	1.390(3)	C32–H32A	0.9500
C14–C15	1.386(3)	C33–C34	1.377(3)
C14–H14A	0.9500	C33–H33A	0.9500
C15–C16	1.378(3)	C34–C35	1.375(3)
C15–H15A	0.9500	C34–H34A	0.9500
C16–C17	1.376(3)	C35–C36	1.388(3)
C16–H16A	0.9500	C35–H35A	0.9500
C17–C18	1.390(3)	C36–H36A	0.9500
N3–Cu1–N1	161.98(6)	C2–C1–H1A	124.6
N3–Cu1–N4	82.52(6)	C1–C2–C3	106.53(17)
N1–Cu1–N4	102.44(6)	C1–C2–H2A	126.7
N3–Cu1–N2	98.76(6)	C3–C2–H2A	126.7
N1–Cu1–N2	82.70(6)	C4–C3–C2	105.93(16)
N4–Cu1–N2	159.48(6)	C4–C3–H3A	127.0
C1–N1–C4	105.95(15)	C2–C3–H3A	127.0
C1–N1–Cu1	142.72(13)	N1–C4–C3	110.69(16)
C4–N1–Cu1	110.00(12)	N1–C4–C5	116.71(16)
N1–C1–C2	110.89(17)	C3–C4–C5	132.51(17)
N1–C1–H1A	124.6	N2–C5–C4	118.24(16)
N2–C5–H5A	120.9	C21–C20–H20A	126.7
C4–C5–H5A	120.9	C19–C20–H20A	126.7
C5–N2–C6	120.84(15)	C20–C21–C22	106.07(17)
C5–N2–Cu1	110.39(12)	C20–C21–H21A	127.0
C6–N2–Cu1	128.75(11)	C22–C21–H21A	127.0
N2–C6–C13	111.52(14)	N3–C22–C21	110.33(16)
N2–C6–C7	112.79(14)	N3–C22–C23	115.78(16)
C13–C6–C7	111.35(14)	C21–C22–C23	133.84(18)
N2–C6–H6A	106.9	N4–C23–C22	117.82(16)
C13–C6–H6A	106.9	N4–C23–H23A	121.1

(*continued*)

Downloaded At: 13:44 23 January 2011

TABLE V Continued

Cu1–N3	1.9442(15)	C17–H17A	0.9500
C7–C6–H6A	106.9	C22–C23–H23A	121.1
C12–C7–C8	118.35(17)	C23–N4–C24	122.11(15)
C12–C7–C6	122.24(17)	C23–N4–Cu1	111.69(12)
C8–C7–C6	119.40(16)	C24–N4–Cu1	126.18(12)
C9–C8–C7	120.55(19)	N4–C24–C31	111.11(15)
C9–C8–H8A	119.7	N4–C24–C25	114.17(15)
C7–C8–H8A	119.7	C31–C24–C25	112.44(15)
C8–C9–C10	120.32(19)	N4–C24–H24A	106.1
C8–C9–H9A	119.8	C31–C24–H24A	106.1
C10–C9–H9A	119.8	C25–C24–H24A	106.1
C11–C10–C9	119.78(19)	C26–C25–C30	119.00(17)
C11–C10–H10A	120.1	C26–C25–C24	122.58(17)
C9–C10–H10A	120.1	C30–C25–C24	118.41(17)
C10–C11–C12	119.79(19)	C25–C26–C27	120.50(19)
C10–C11–H11A	120.1	C25–C26–H26A	119.7
C12–C11–H11A	120.1	C27–C26–H26A	119.7
C11–C12–C7	121.20(18)	C28–C27–C26	120.42(19)
C11–C12–H12A	119.4	C28–C27–H27A	119.8
C7–C12–H12A	119.4	C26–C27–H27A	119.8
C18–C13–C14	118.77(18)	C27–C28–C29	119.60(19)
C18–C13–C6	122.80(16)	C27–C28–H28A	120.2
C14–C13–C6	118.25(16)	C29–C28–H28A	120.2
C15–C14–C13	120.71(18)	C30–C29–C28	120.1(2)
C15–C14–H14A	119.6	C30–C29–H29A	119.9
C13–C14–H14A	119.6	C28–C29–H29A	119.9
C16–C15–C14	120.05(19)	C29–C30–C25	120.31(19)
C16–C15–H15A	120.0	C29–C30–H30A	119.8
C14–C15–H15A	120.0	C25–C30–H30A	119.8
C17–C16–C15	119.76(19)	C32–C31–C36	118.63(18)
C17–C16–H16A	120.1	C32–C31–C24	122.65(17)
C15–C16–H16A	120.1	C36–C31–C24	118.59(18)
C16–C17–C18	120.48(19)	C31–C32–C33	120.5(2)
C16–C17–H17A	119.8	C31–C32–H32A	119.8
C18–C17–H17A	119.8	C33–C32–H32A	119.8
C13–C18–C17	120.21(18)	C34–C33–C32	120.6(2)
C13–C18–H18A	119.9	C34–C33–H33A	119.7
C17–C18–H18A	119.9	C32–C33–H33A	119.7
C19–N3–C22	106.33(15)	C35–C34–C33	119.3(2)
C19–N3–Cu1	141.19(13)	C35–C34–H34A	120.3
C22–N3–Cu1	112.12(12)	C33–C34–H34A	120.3
N3–C19–C20	110.63(17)	C34–C35–C36	120.2(2)
N3–C19–H19A	124.7	C34–C35–H35A	119.9
C20–C19–H19A	124.7	C36–C35–H35A	119.9
C21–C20–C19	106.63(17)	C31–C36–C35	120.7(2)
C31–C36–H36A	119.7		
C35–C36–H36A	119.7		
N1–Cu1–N2/N3–Cu1–N4	29.3		

showed an analogous shift of ca. 50 cm^{-1}. There does not appear to be a correlation between the steric bulk of the R group and the shift of ν(C=N) relative to the free Schiff base. The lowest energy value of ν(C=N) occurs for **1a**, at 1574 cm^{-1}, but we do not know the shift because the precursor Schiff base has not been isolated as a stable compound. From Table VI, however, the comparison of the C=N distances for the four structurally characterized complexes shows that for **1d**, **1e**, and **1f** the C=N distances are all within the range 1.28(2) to 1.292(2) Å, which is within experimental uncertainty, whereas the value for **1a** is clearly longer at 1.328(14) Å,

Downloaded At: 13:44 23 January 2011

TABLE VI Comparison of average metal-ligand and selected intraligand interatomic distances (Å) and dihedral angles from crystal structures of four pyrrolate-imine copper(II) complexes

Identifier	$Cu–N_{pyrr}$	$Cu–N_{im}$	$C=N$	$C_{im}–C_{pyrr}$	$C_{pyrr}–N_{pyrr}$	*Dihedral angle* (°)
1a	1.950(8)	1.972(9)	1.328(14)	1.406(16)	1.360(12)	0
1g	1.951(2)	2.024(2)	1.292(2)	1.414(3)	1.368(2)	29.3
1f	1.959(2)	2.038(2)	1.290(2)	1.421(3)	1.373(3)	33.2
1d	1.939(8)	2.054(8)	1.28(2)	1.42(2)	1.42(2)	61.3

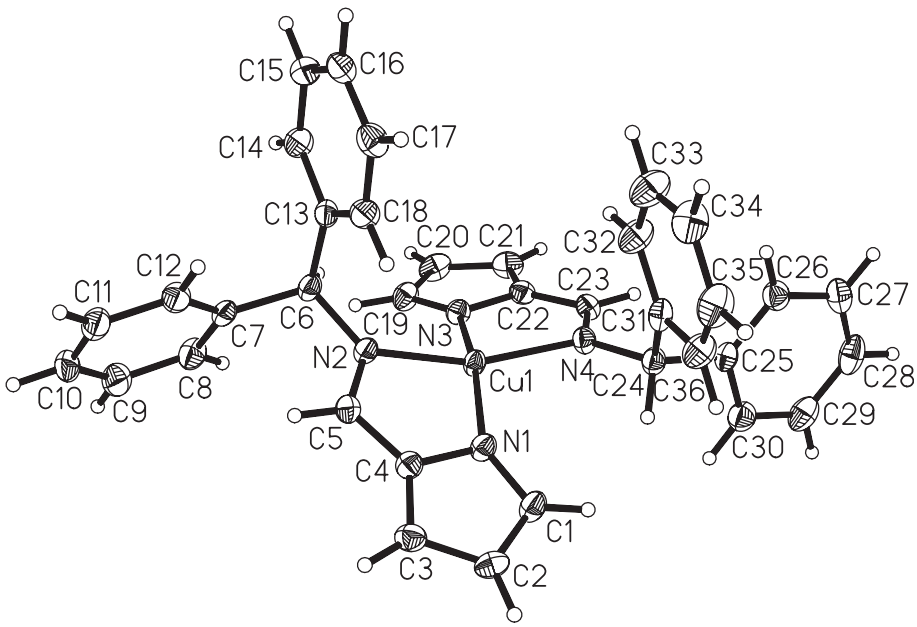

FIGURE 5 Structure of **1g** showing atom numbering scheme.

and well outside the error range of the comparison. It is reasonable to infer that this longer bond length in **1a** is consistent with the observed ν(C=N) being at least 16 cm^{-1} lower in energy than the other complexes listed in Table VII.

All other complexes, except for the 1-adamantyl variant **1e**, show ν(C=N) in the range 1590 to 1597 cm^{-1}, whereas ν(C=N) for **1e** occurs at 1583 cm^{-1}. It is perhaps noteworthy that the difference between the 1-adamantyl derivative **1e** and the 2-adamantyl counterpart **1h** is 14 cm^{-1}, which is comparable to the 16 cm^{-1} difference between **1a** and **1f**, and possibly reflects a slight difference in the respective C=N bond lengths in these complexes. As a caveat to possible over-interpretation, it is notable that although **1e** and **1d** have slightly different ν(C=N) their visible and EPR spectral features (Tables III and VII) are almost identical.

Upon comparison of pertinent crystal data (Table VI), one emergent trend is that the average Cu–N(imine) bond length increases slightly and incrementally as the dihedral angle increases, as seen in the values 1.972(9) Å for **1a** compared with 2.054(8) Å for **1d**. In contrast, the Cu–N(pyrrolate) distance is close to 1.950 Å for all complexes, without a trend with respect to the geometry of the complex. Intraligand distances other

Downloaded At: 13:44 23 January 2011

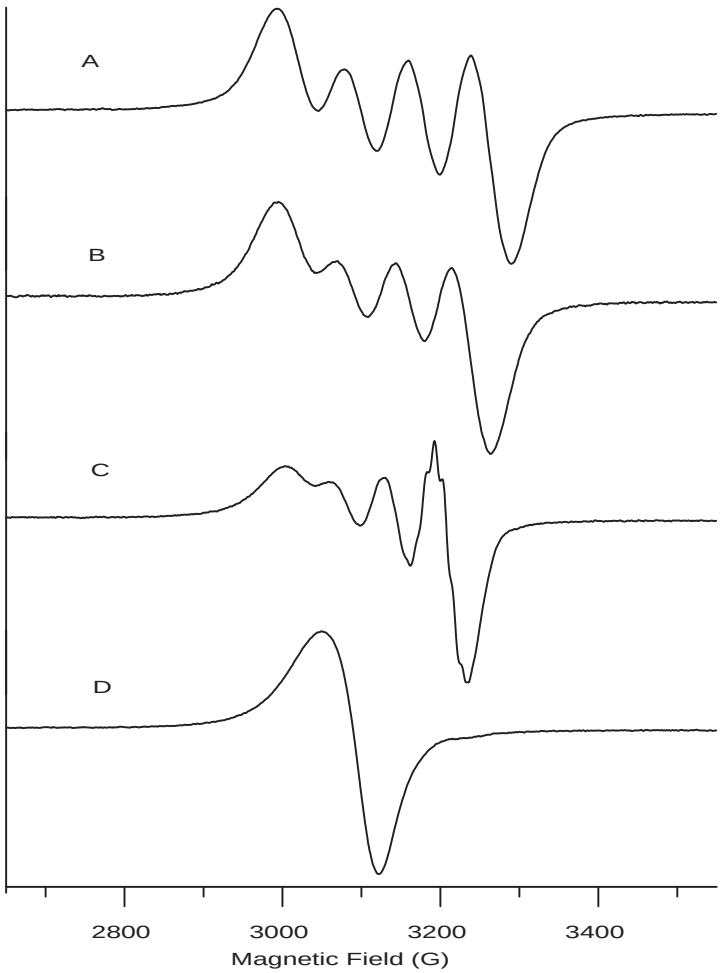

Downloaded At: 13:44 23 January 2011

FIGURE 6 Fluid solution X-band EPR spectra. A, **1a**, R = H; B, **1b**, R = CH_3; C, **1h**, R = 2-adamantyl; D, **1e**, R = 1-adamantyl.

TABLE VII EPR parameters for **1a**–**1h**[a]

Identifier	*R*	g_{iso}	g_z	A_{iso} (10^{-4} cm^{-1})	A_z (10^{-4} cm^{-1})	*Dihedral angle*[b] (°)	*Dihedral angle*[c] (°)
1a	H	2.096	2.190	75	208	0[1]	
1b	CH_3	2.104	2.205	67	193		13–16
1c	*n*-Butyl	2.106	2.212	59	178		25–29
1f	Benzyl	2.107	2.212	58	180	33.2	
1g	Diphenylmethyl	2.109	2.218	56	178	29.3	
1h	2-Adamantyl	2.111	2.222	58	174		35–37
1d	*tert*-Butyl	2.141	2.280	18	110	61.3[2]	
1e	1-Adamantyl	2.140	2.277	18	110		60–61

[a]Samples listed in same order as in Table III; [b]The dihedral angle N_{im}–Cu–N_{pyrr} / N_{im}–Cu–N_{pyrr} between the two chelate rings (N_{im} is imine nitrogen, N_{pyrr} is pyrrolate) obtained from X-ray crystal structure; [c]The dihedral angle N_{im}–Cu–N_{pyrr} / N_{im}–Cu–N_{pyrr} between the two chelate rings estimated from the correlation between EPR parameters and the dihedral angles from crystal structures, see text.

than the C=N distance described above show little variation over the range of structures. These observations together are entirely consistent with the changes expected as the imine R group increases in steric bulk. Essentially constant metal–ligand and intraligand bond distances were also seen in the two 2-amino-1-cyclopentenedithiocarboxylato N_2S_2 complexes cited by Bereman and co-workers [9], although those examples differed in having internal strain and not steric bulk of substituent as the distorting force in the coordination sphere, as well as having a relatively small difference in dihedral angle in the two complexes (52.8° *vs.* 57.1°).

The decrease in A_z with increasing dihedral angle can be seen in Fig. 7, spectra A through D, the proton, methyl, 2-adamantyl, and 1-adamantyl derivatives. The superhyperfine interactions also diminish, in the same order. In a similar vein, for three related N_2S_2 complexes, loss of superhyperfine was rationalized by Bereman [9] in terms of increasing dihedral angle rotating the metal–nitrogen bonds out of alignment

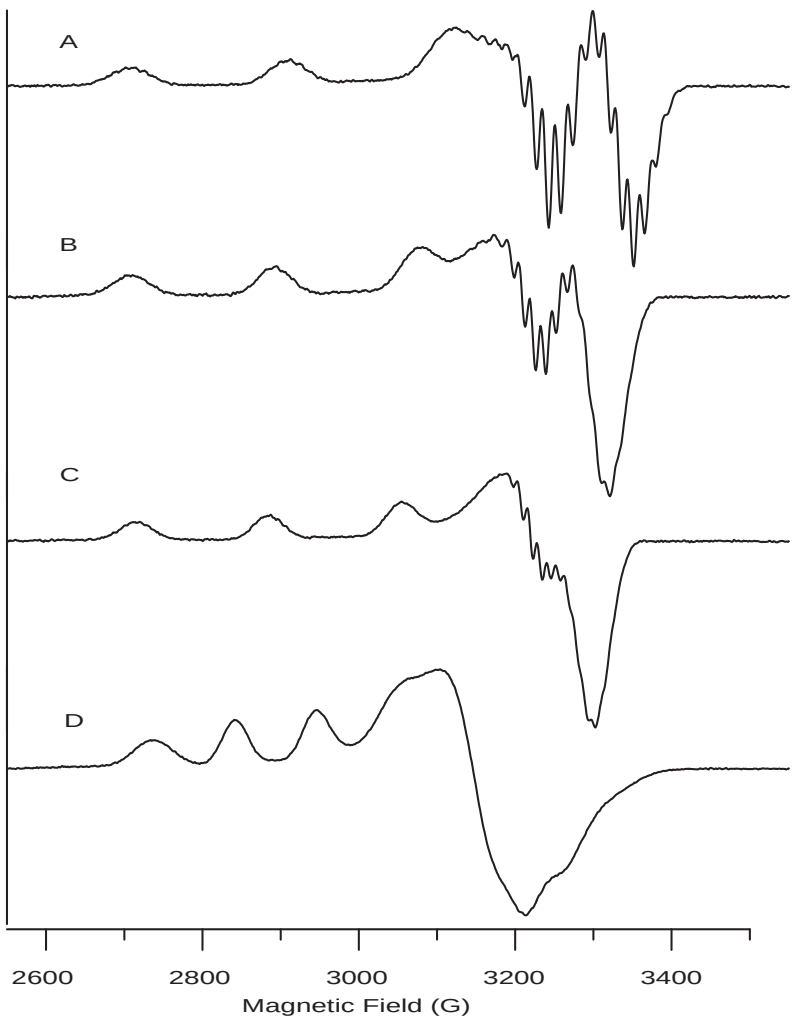

FIGURE 7 X-band EPR spectra at 100 K in 2 : 1 toluene : chloroform glass. A, **1a**, R = H; B, **1b**, R = CH_3; C, **1h**, R = 2-adamantyl; D, **1e**, R = 1-adamantyl.

Downloaded At: 13:44 23 January 2011

with the Cu(II) ground-state orbital, thereby diminishing the overlap between the unpaired electron and the nitrogen atom nucleii.

Yokoi and Addison [6] noted that the slopes of plots of A_z *vs.* g_z for copper complexes were similar for a wide range of complexes. Our data for the pyrrole-2-carboxaldimines complexes fit with their trend. Our data also fit with their inverse correlation between the energy of the ligand-field transition and g_z. Our points for g_z for **1f** and **1g** fit nicely on their line for the correlation between g_z and the dihedral angle between the ligand planes [6]. When the EPR parameters for the complexes that had not been crystallographically characterized (**1b**, **1c**, **1h**, and **1e**) were compared with the trends in g_{iso}, g_z, A_{iso}, and A_z as a function of dihedral angle, the dihedral angles listed in Table VII were estimated. For these complexes the dihedral angles increase from about 15° for R = CH_3 to about 27° for R = *n*-butyl. While **1h** is reasonably considered to be pseudo-planar, its 1-adamantyl counterpart, and isomer, **1g**, is pseudo-tetrahedral with a calculated dihedral angle of 61°. This difference is attributed to the different orientations of the adamantyl substituents on the imine nitrogen giving rise to different steric effects: the 1-adamantyl binds via a tertiary carbon, but the 2-adamantyl binds via a secondary carbon.

Downloaded At: 13:44 23 January 2011

It is perhaps surprising that the X-ray crystal structure of the diphenylmethyl analog **1g** shows a smaller dihedral angle than its smaller benzyl counterpart. Further inspection (Table V) shows that pertinent intramolecular distances for **1g** around the imine nitrogen atom are slightly elongated compared to analogous distances in **1f**, probably from steric repulsions between the phenyl rings within the diphenylmethyl substituent itself. For example, the nitrogen-to-carbon bond length N7–C8 is 1.456(3) Å in **1f** (Table IV), whereas the analogous N2–C6 distance is 1.476(2) Å in **1g** (Table V). Distances around the methylene carbon are also slightly longer: for instance, C8–C9 is 1.517(3) Å in **1f**, and C6–C7 is 1.524(2) Å in **1g**. It is proposed that the presence of a second phenyl ring in the R group of **1g** *vs.* **1f** yields more potential intermolecular attractive packing forces (through possible ring stacking) whose presence within the crystal is able to overcome possible intramolecular steric repulsions. The outcome is a slightly smaller dihedral angle for **1g** than for **1f**.

For copper(II) complexes the ligand-field transition energy decreases as tetrahedral distortion increases [6]. On the basis of peaks at 18 900, 18 200, and 18 100 cm^{-1}, respectively, as well as the shoulders at 14 600, 14 300, and 14 200 cm^{-1}, the electronic absorption spectra for **1f–1h** (Table III) in $CHCl_3$ solution are consistent with dihedral angle increasing in the order benzyl < diphenylmethyl < 2-adamantyl. As just discussed, the structurally observed dihedral angles (Table VI) give the reversed order of benzyl > diphenylmethyl, suggesting that in solution the absence of crystal packing forces "releases" the diphenylmethyl group to exert greater steric effects than its benzyl counterpart, which gives rise to a larger dihedral angle than for the benzyl complex. The EPR parameters (Table VII) for the diphenylmethyl and benzyl derivatives are within experimental uncertainty, indicating geometries in solution that are more similar than the structures in the crystals. For each of the plots of EPR parameters as a function of dihedral angle, the point for the diphenyl derivative deviated slightly from the line, in the direction that would be consistent with a dihedral angle in solution that is larger than in the crystal.

In summary, estimation of the dihedral angle was made for four complexes based on correlations of EPR parameters with dihedral angles from four related complexes of known structure. For the series **1a–1h**, a smoothly increasing dihedral angle is inferred

from the measurements of decreasing A_z, increasing g_z, and red-shifted ligand-field taken together for all complexes except **1g**. The ranking of the substituents in terms of increasing steric size in solution thus follows: H < Me < *n*-butyl ~ benzyl < diphenylmethyl < 2-adamantyl < *tert*-butyl ~ 1-adamantyl. The anomalous behavior of **1g** is attributed to enhanced crystal packing forces that appear to give rise to a smaller than expected dihedral angle. A knowledge of the geometries of these complexes is expected to be of relevance in future studies aimed at exploring the reactivity of **1a–1h** with potential ligands such as peroxide, superoxide, and thiolates.

Acknowledgments

Stephen Fox wishes to thank Dr. Neil R. Brooks and Dr. Victor G. Young, Jr. of the University of Minnesota X-Ray Crystallographic Laboratory for the crystal structure determinations; the Louisiana Board of Regents Support Fund (grant # (1998-01)-RD-A-22) for funding this work, for summer salary support for S.F., and for stipend support for C.M.W.; and the Howard Hughes Foundation for an Undergraduate Award to J.L.S.. G.R.E. and S.S.E. acknowledge NIH grant GM21156 for support of this work.

Downloaded At: 13:44 23 January 2011

References

[1] R. Tewari and R.C. Srivastava, *Acta Crystallogr., Sect. B*, **27**, 1644 (1971).
[2] C.H. Wei, *Inorg. Chem.* **11**, 2315 (1972).
[3] T. Kikuchi, C. Kabuto, H. Yokoi, M. Iwaizumi and W. Mori, *J. Chem. Soc., Chem. Commun.* 1306 (1983).
[4] A. Chakravorty and T.S. Kannan, *J. Inorg. Nucl. Chem.* **29**, 1691 (1967).
[5] R.H. Holm, A. Chakravorty and L.J. Theriot, *Inorg. Chem.* **5**, 625 (1966).
[6] H. Yokoi, A.W. Addison, *Inorg. Chem.* **16**, 1341 (1977).
[7] R.J. Dudley, R.J. Fereday, B.J. Hathaway and P.G. Hodgson, *J. Chem. Soc., Dalton Trans.* 882 (1972).
[8] D.J. Patmore, D.F. Rendle, A. Storr and J. Trotter, *J. Chem. Soc., Dalton Trans.* 718 (1975).
[9] R.D. Bereman, G.D. Shields, J. Bordner and J.R. Dorfman, *Inorg. Chem.* **20**, 2165 (1981).
[10] N.M. Atherton, Electron Spin Resonance (Halsted Press, New York, 1973), p. 108–114.
[11] A.D. Toy, S.H.H. Chaston, J.R. Pilbrow and T.D. Smith, *Inorg. Chem.* **10**, 2219 (1971).
[12] An empirical correction for absorption anisotropy, R. Blessing, *Acta Crystallogr., Sect A* **51**, 33 (1995).
[13] SAINT V6.1, Bruker Analytical X-Ray Systems, Madison, WI.
[14] SHELXTL-Plus V5.10, Bruker Analytical X-Ray Systems, Madison, WI.
[15] H. Brunner, B. Nuber and T. Tracht, *Tetrahedron: Asymmetry* **9**, 3763 (1998).
[16] P. Pfeiffer, T. Hesse, H. Pfitzinger, W. Scholl and H. Thielert, *J. Prakt. Chem.* **149**, 217 (1937).
[17] A. Mohamadou and J.-P. Barbier, *Inorg. Chim. Acta.* **169**, 17 (1990).